ELSEVIER

Contents lists available at ScienceDirect

International Journal of Biological Macromolecules

journal homepage: www.elsevier.com/locate/ijbiomac





Development of pullulan/chitosan/salvianolic acid ternary fibrous membranes and their potential for chemotherapeutic applications

Salahuddin Ahmed ^a, Megan Keniry ^b, Victoria Padilla ^a, Narcedalia Anaya-Barbosa ^a, Md Noushad Javed ^a, Robert Gilkerson ^b, Kithzia Gomez ^a, Ali Ashraf ^a, Acharan S. Narula ^c, Karen Lozano ^{a,*}

- ^a Department of Mechanical Engineering, The University of Texas Rio Grande Valley, Edinburg, TX, USA
- ^b Department of Biology, The University of Texas Rio Grande Valley, Edinburg, TX, USA
- ^c Narula Research, Chapel Hill, NC, USA

ARTICLE INFO

Keywords: Salvianolic acid B Nanofiber Forcespinning Anticancer

ABSTRACT

This study investigates the feasibility of centrifugal spinning for producing fibrous membranes containing pullulan, chitosan, and danshen extract. The danshen extract is composed of 20 wt% salvianolic acid B (SA). Citric acid was added to the mixture as a crosslinking agent to promote its use in the aqueous medium. The influence of the danshen concentration (25 wt% and 33 wt%) on fiber morphology, thermal behavior, and the biochemical effect was analyzed. Developed fiber-based membranes consist of long, continuous, and uniform fibers with a sparse scattering of beads. Fiber diameter analysis shows values ranging from 384 \pm 123 nm to 644 \pm 141 nm depending on the concentration of danshen. The nanofibers show adequate aqueous stability after crosslinking. Thermal analysis results prove that SA is loaded into nanofibers without compromising their structural integrity. Cell-based results indicate that the developed nanofiber membranes promote cell growth and are not detrimental to fibroblast cells. Anticancer studies reveal a promising inhibition to the proliferation of HCT116 colon cancer cells. The developed systems show potential as innovative systems to be used as a bioactive chemotherapeutic drug that could be placed on the removed tumor site to prevent development of colon cancer microdeposits.

1. Introduction

Targeted drug delivery systems can increase the therapeutic effect of the drug and limit the adverse consequences to non-targeted locations. Nanotechnology-based drug delivery methods, such as nanoparticles [1], hydrogels [2], and nanofibers [3,4], are gaining attention due to their potential to deliver therapeutics at a specific site with a precise pharmacokinetic profile. Nanofiber based membranes have recently gained attention as a viable medium for targeted drug delivery. These membranes possess unique characteristics such as high surface area, controllable porosity, and ease of handling. Nanofibers have proven potential for delivering both hydrophilic and hydrophobic drugs [5,6]. Nanofiber systems offer unique ways to increase the rate of dissolution of poorly soluble substances, which reduces the drawbacks of oral bioavailability [7]. Additionally, nanofibers can i) improve effectiveness of loaded drug, ii) enable encapsulated drugs to maintain their therapeutic effect for extended periods by shielding drugs from adverse

atmospheric conditions, and iii) provide protection to sensitive biological molecules from environmental damage. Xie et al. [8] developed anticancer drug paclitaxel-loaded PLGA nanofibers; the system contained the drug in a solid-state solution within polymeric micro and nanofibers. A steady drug release was demonstrated for 60 days. Guimares et al. [9] developed PLGA-daunorubicin nanofiber membranes with enhanced cytotoxicity against A431 tumor cells, the same level of cytotoxicity against fibroblast cells was maintained when compared to free daunorubicin. Han et al. [10] developed PCL core-PEO sheath enzyme nanofibers containing toxin-mitigating diisopropylfluorophosphatase (DFPase). The nanofiber provided protection to sensitive biological molecules from environmental damage.

Fig. 1a shows the chemical structure of pullulan (PL), a commercially available biopolymer grown by yeast-like fungus called *Aureobasidium pullulans*, it grows in sugar and starch cultures [11,12]. It is formed on the surface of microbial cells as an amorphous slime [13–16]. It is neither toxic, nor immunogenic or mutagenic [17]. It is a linear,

E-mail address: karen.lozano@utrgv.edu (K. Lozano).

^{*} Corresponding author.

unbranched water-soluble exopolysaccharide ((C₆H₁₀O₅)_n). The molecular weight of pullulan ranges from 4.5×10^4 to 6×10^5 Da, and is heavily influenced by cultivating parameters [11]. It has maltotriose repeating units, which are connected by α -(1,6) glycosidic bonds [18]. Two glucose molecules inside maltotriose are linked by a α -(1,4)glycosidic bond [19]. It is available as a white powder that dissolves easily in hot and cold water and diluted alkali mediums. Pullulan is not soluble in most organic solvents with the exception of dimethylsulfoxide and formamide [20]. Due to its unique physico-chemical properties, pullulan is used in food [21], pharmaceutical [22], and biomedical applications. Its inertness, biocompatibility, low oxygen permeation, and mechanical and chemical characteristics make pullulan attractive for biomedical applications such as targeted drug [23] and gene [24] delivery, medical imaging [25], vaccination [26], tissue engineering [27], and wound dressing [28]. Additionally, the FDA has declared pullulan a safe system and has received a GRAS designation [29]. Chitosan (CS), Fig. 1b, is a modified natural, biodegradable, biocompatible, non-toxic homopolymer of linear nitrogenous polysaccharides [30]. Commercial CS is produced by deacetylating chitin, a naturally occurring polysaccharide, which is the structural component of the exoskeleton of crustaceans [31]. It is composed of randomly distributed β -(1 \rightarrow 4)-linked N-acetyld-glucosamine (GlcNAc) and d-glucosamine (GlcN) (Fig. 1b), the latter of which gives it cationic properties at physiological pH. It has an average molecular weight ranging between 3800 and 20,000 Da [32]. A variety of CS derivatives have been created using free amino and hydroxyl groups with increased solubility, which makes CS an attractive compound in pharmaceutical and biomedical processes, such as gene/ vaccine/drug delivery [33], tissue engineering [34], wound healing [35], and manufacture of cosmetic products. Pullulan/Chitosan composites have shown promising applications in targeted drug delivery and

tissue engineering. Xu et al. [36] developed a ternary nanofiber scaffold composed of chitosan, pullulan, and tannic acid as the therapeutic compound. The developed scaffold was highly stable in water, exhibited antibacterial characteristics, improved cell proliferation and attachment, and non-cytotoxic behavior to fibroblast cells. Barbosa et al. [37] developed nanofibrous membranes composed of citric acid, pullulan, aloe vera extract, and chitosan. A synergistic antibacterial activity against E. coli and ability to promote cell adhesion and proliferation was reported. Pullulan/chitosan composites have the potential to be used for chemotherapeutic applications. Liang et al. [38] used oxidized pullulan with chitosan-grafted-dihydrocaffeic acid to develop pH-sensitive, mucosal adhesive and multifunctional injectable hydrogels for localized drug carriers. The hydrogel showed a slow prolonged release of anticancer or antibacterial drugs for the treatment of colon cancer. Pullulan/chitosan nanofiber membranes have shown potential in wound dressing and skin tissue engineering. Fard et al. [39] developed pullulan chitosan based nano emulsion for effective drug delivery to the A375 cells.

Salvianolic acid B (SA), Fig. 1c, is a bioactive component derived from the Chinese medicinal herb, Danshen, which is the dry root of *Saliva miltiorrhiza*. It is defined as a super herb due to its low toxicity and has been widely used in Chinese pharmacology to treat cardiovascular diseases such as angina pectoris, myocardial infarction and stroke [40-42]. Salvianolic acid B consists of three parts of Danshensu $(\underline{C_9H_{10}O_5})$ and one part of dimeric caffeic acid. It has been clinically used to treat pulmonary fibrosis, cardiovascular diseases (CVDs), malignant tumors, cerebrovascular diseases, and chronic wounds by stimulating angiogenesis, re-epithelialization, and cell proliferation [43,44]. It has shown various anti-oxidative [45] and anti-inflammatory [46] effects in different disease models. Treatment with Salvianolic acid B

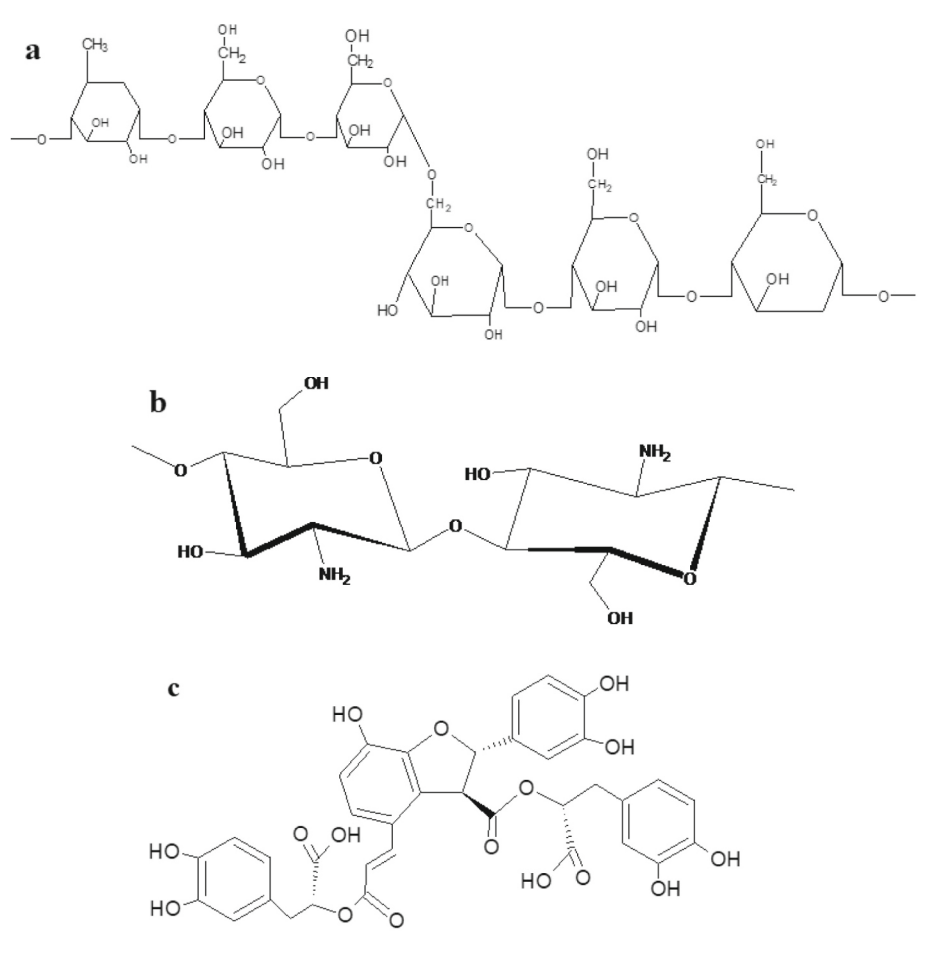


Fig. 1. Chemical structure of pullulan (a), chitosan (b), salvianolic acid B (c).

improved motor function [47] and reduced brain damage [48] after cerebral ischemia in rats. Chen et al. [42] reported that Salvianolic acid attenuates brain damage and inflammation following the traumatic brain injury in rats. Liang et al. [49] reported that Salvianolic acid B serves as a matrix metalloproteinase inhibitor, which is helpful in the healing of chronic wounds. Studies suggest that Salvianolic acid inhibits cancer initiation and development, and its anticancer effect has been demonstrated in both in vivo and in vitro model [50,51]. Zhou et al. [52] reported that Salvianolic acid B protects various cells, including nerve cells and hepatocytes, by acting as an antioxidant and scavenger of free radicals. Despite having several biological activities, due to its low efficacy, poor systemic delivery, and low bioavailability, the extensive use of SA has been limited [53]. Nanotechnology-based targeted drug delivery systems have been proven to be able to overcome these limitations and improve the bioactivity of Salvianolic acid B [54]. Li et al. [53] developed Salvianolic acid loaded phospholipid complex nanoparticles that are more potent than free Salvianolic acid and had an anticancer effect against HNSCC cells. Shoba et al. [55] developed a nanofibrous membrane for wound dressing with salvianolic acid and bromelin that improved keratinocyte cell growth, endothelial cell migration, vessel density, neovascularization, and inhibited bacterial growth. Kuang et al. [56] developed internal layer of artificial vascular grafts with SA and heparin that showed sustained release of Salvianolic acid and heparin for 30 days without any burst release.

Colorectal cancer (CRC) is the third most common type of cancer in the world. Even though CRC treatment has come a long way in recent years, it is still the third leading cause of cancer deaths in the United States and the fourth leading cause of cancer deaths worldwide [57,58]. 5-Fluorouracil (5-FU) and its derivatives are currently used for the initial chemotherapy of CRC [59,60]. Even though most patients respond well to this chemotherapy, the relapse rate is still high because of the growing level of resistance to the chemotherapeutic agents [61]. It has become crucial to find new chemotherapeutic drugs. Salvianolic acid has been shown to effectively reduce multidrug resistance (MDR) in HCT116 colon cancer cells by inhibiting the expression of CD44, SOX2, and ABCG proteins [62]. Jing et al. [61] reported that Salvianolic acid B is an autophagy inducer with potent anticancer activity as a single agent by inducing autophagic cell death in HCT116 CRC cells.

Although SA-loaded nanofibers have been reported previously, to the knowledge of the authors, the study of SA-loaded nanofibers for anticancer studies has not yet been reported. In this study, SA-loaded PL-CS composite nanofiber membranes were developed using the forcespinning® method to avoid the use of electric fields and organic solvents. The forcespinning approach has demonstrated high yield and proven potential to scale up. The influence of SA concentrations and processing parameters on the morphological and thermophysical properties of developed nanofiber membranes was investigated. The results indicate that nanofibers produced by forcespinning can include SA and exhibit structural integrity suitable for prospective usage as bioactive agent delivery systems. The in vitro cell viability studies and in vitro anticancer properties were evaluated.

2. Materials and experimental methods

2.1. Materials

Pullulan (CAS 9057-02-7) was purchased from Tokyo Chemical Industry Co. (Japan). Chitosan (CAS 9012-76-4) with a low–molecular weight (MW =50,000–190,000 and 75 %–85 % degree of deacetylation) was purchased from Sigma–Aldrich (St Louis, USA). Citric acid was purchased from Sigma Aldrich (St Louis, USA). Deionized (DI) water was produced from a Smart2Pure water purification system. Danshen extract containing 20 % Salvianolic acid B was acquired from Jiaherb Phytochem (China). This bioactive compound will be identified as SA throughout the manuscript. All of the chemicals were used in analytical grade without any further purification. As for fiber production, the 30-

gauge bevel needles from PrecisonGlideTM were obtained from Fisher Scientific.

2.2. Solution preparation

300 mg of citric acid (CA) was added to 10 ml of deionized water (DI). The mixture was homogenized at 600 rpm using a magnetic stirrer (Thermo Scientific, Cimarec+ series) for 30 min. 50 mg of chitosan (CS) was added to the CA solution. The solution was left on the magnetic stirrer overnight at 800 rpm for homogenization. 2.2 g of pullulan (PL) was added to the mixture to prepare the control (PL-CS) solutions. Three control solutions were prepared. Then, SA was added to the control samples to prepare 25 wt% and 33 wt% of solutions identified as PL-CS-SA(L) to identify the low concentration of SA and PL-CS-SA(H) for the high concentration of SA. The mixtures were stirred overnight to prepare homogeneous solutions.

2.3. Development of nanofiber

The nanofiber membranes were developed using centrifugal force in Cyclone-1000 M (FiberRio Technology Corp, McAllen, USA), which consists of a cylindrical spinneret with two nozzles. A 3 ml syringe was used to inject 2 ml of the prepared solution into the spinneret. Spinning was carried out for six minutes at 6500 rpm at ambient temperature and 20–30 % relative humidity. Mats from five spinning cycles were collected manually using a 10 cm \times 10 cm hollow frame and stored in sealed bags containing desiccants for moisture control.

2.4. Crosslinking of nanofiber

Following the collection of nanofibers, the membranes were placed in an oven and heated to 140 $^{\circ}$ C in a vacuum environment for 1 h and 15 min for crosslinking to take place. The composite nanofibers became stable in water after crosslinking process. The samples were then taken out of the oven and allowed to cool down before further analysis.

2.5. Characterization

The surface morphology of the nanofibrous membranes was examined using a field-emission scanning electron microscope (FESEM) (Sigma VP, Zeiss Evo LS10, Jena, Germany). A voltage of 1 kV was applied throughout the procedure, with magnifications ranging from $35\times$ to $15,000\times$. The images were analyzed using ImageJ software (Version-1.8.0) to determine the average fiber diameter. The average fiber diameter was obtained by measuring the fiber diameter of 100 different fibers.

The Fourier transform infrared (FTIR) spectra were obtained using a Nicolet iS5 spectrometer in the attenuated total reflection (ATR) mode. Samples of 1 cm \times 1 cm were cut and placed in the FTIR machine. 16 scans were collected in the range of 400–4000 cm $^{-1}$ with a resolution of 4 cm $^{-1}$.

The X-ray powder diffraction (XRD) patterns of the SA powder and SA loaded nanofibers were recorded with a Bruker D2 Phaser X-ray diffractometer under a wavelength of 2θ range from 10° to 75° in with a step of 0.05° , with 5 s counting time. X-ray photoelectron spectrometry (XPS) was obtained using a Thermo Scientific K α XPS surface analysis instrument with a micro-focused monochromated Al K- α X-ray source at 1 eV for scans and 1 keV for depth analysis with an etching rate of 1 nm/s.

The thermal properties were analyzed using thermogravimetric analysis (TGA). TGA was carried out using Netzsch 209. For the analysis, 10 mg samples were heated from 27 $^{\circ}\text{C}$ to 700 $^{\circ}\text{C}$ at a heating rate of 10 $^{\circ}\text{C/min}$ in a nitrogen environment.

2.6. In vitro drug release studies

The kinetics of SA release were evaluated by submerging a 50-mg loaded nanofiber scaffold into 10 ml of PBS solution at pH 7.4. At predetermined time points, 3 ml of phosphate-buffered saline (PBS) were drawn and stored in a vial. The nanofiber loaded PBS solution was replenished with 3 ml of fresh PBS solution. The release profile of SA was analyzed at 282 nm using a UV spectrometer (Cary60, Agilent Technology, Santa Clara, CA). The cumulative release study was conducted over the course of 4 days. The encapsulation efficiency of drug loaded nanofiber was measured by dissolving the uncrosslinked nanofiber in PBS and measuring the absorbance using the UV–vis spectrometer.

2.7. Cell viability study

35,000 3T3 mouse embryonic fibroblasts were seeded to a 24-well plate in the presence of the nanofiber materials (20 mg) using Dulbecco's modified Eagle's medium (DMEM) with 10 % fetal bovine serum (FBS) and 5 % antifungal/antibacterial (Anti/Anti, Thermo Fisher, Waltham, MA, USA) and incubated for two days at 37 °C and 5 % CO2 environment. The cell proliferation and viability were assessed using the Trevigen TACS MTT Cell Proliferation Assay Kit (Gaithersburg, MD). MTT Reagent (50 μ l) was added to each well and incubated for 4 h at 37 °C and 5 % CO2. Media was aspirated, and 200 μ l DMSO reagent was added, and incubation was continued for an additional 4 h. MTT signal was detected at A_{595} using a Bio-Rad iMark microplate reader.

2.8. Invitro anticancer studies

To determine the anticancer effect of SA embedded with the nanofibers, in vitro cytotoxicity testing was carried out using human colon cancer HCT116 cell lines. 12,000 cells were seeded along with nanofiber (20 mg) per well in 24-well plates using Dulbecco's modified Eagle's medium (DMEM) with 10 % fetal bovine serum (FBS) and 5 % antifungal/antibacterial (Anti/Anti, Thermo Fisher, Waltham, MA, USA). Cells were grown under standard tissue culture conditions (5 % CO $_2$ and 37 °C) for five days. The effect of human cell proliferation and/or viability was assessed using the Trevigen TACS MTT Cell Proliferation Assay Kit (Gaithersburg, MD). Each well contained fifty microliters of MTT reagent and was incubated for four hours at 37 °C and 5 % CO $_2$. Finally, 200 μL of DMSO reagent was added, and incubation was continued for an additional 4 h. The optical density (A $_{595}$) was measured using a Bio-Rad iMark microplate absorbance reader. Samples were carried out in triplicate.

2.9. In vitro apoptosis study

In vitro apoptosis study was conducted using the method described by Ahmed et al. [63]. In short, the growth medium of the cells was removed following treatment. The cells were subjected to incubation with a 0.25 % trypsin solution at a volume of 2 ml per sample for a duration of 5 min at ambient temperature. A volume of 1.5 ml from each plate was transferred into microcentrifuge tubes with a capacity of 1.7 ml. The tubes were then subjected to centrifugation at a force of Gx0.2 for a duration of 10 min. The Trypsin supernatant was removed, and the cells were subsequently resuspended in PBS. Following this, the cells were centrifuged at Gx0.2 for a duration of 10 min. The supernatant of PBS was removed and the cells were subsequently resuspended in a diluted binding buffer obtained from the Molecular Probes FITC Annexin V/Dead Cell Apoptosis Kit, (Thermo Fisher in Waltham, MA). A volume of $100 \,\mu l$ of each sample was diluted using a binding buffer and subsequently introduced into a new microcentrifuge tube. In each tube, $2~\mu l$ of Annexin V FITC and $1~\mu l$ of PI were introduced and allowed to incubate for 15 min in a dark environment. After a 15-min incubation period, 400 µl of binding buffer were introduced and cellular samples were subjected to sorting via the BD FACS Celesta flow cytometer (BD

Biosciences, San Jose, CA).

3. Results and discussions

Forcespinning® technology was chosen due to its ability to produce a high yield of nanofibers. Various concentrations of PL-CS-SA solutions were prepared to produce nanofiber. After optimization process, 18 wt% of PL was selected considering a balance between fiber production yield and fiber diameter. SA-loaded PL-CS systems were developed with SA concentrations ranging from 1 to 50 % (1, 3, 5, 15, 20, 25, 33, and 50 wt %). The optimal rpm for fiber production was found to be 6500. Samples with 25 and 33 wt% of SA were selected for further morphological and thermophysical analysis. SEM images and statistical analysis of the diameter of the developed fiber samples are depicted in Fig. 2. The developed nanofibers have a long, uniform, and continuous fiber morphology with a sparse scattering of beads. The control PL-CS sample has the highest mean fiber diameter, 644 nm, with a standard deviation of 141 nm. With the increasing amount of SA the average fiber diameter decreases. The sample PL-CS-SA(H) has the lowest mean fiber diameter, 385 nm, with a standard deviation of 122.85 nm. With the increase in the concentration of SA, the number of beads increases in the system (supplemental S2). The fluorescent microscopy (supplemental S1) results reveal that SA is concentrated in the nanofibers' beads. With the increasing amount of SA, bead size increased, which resulted in a decrease in the diameter of the nanofiber.

FTIR analysis was carried out to identify different functional groups and interactions between PL, CS, and SA. Fig. 3(a) depicts the FTIR spectra of SA, pullulan, and chitosan, and 3(b) shows the FTIR spectra of the PL-CS control sample, and SA-loaded PL-CS nanofibers. Regarding the SA, CS and PL spectrum (Fig. 3a), bands show strong similarity given their polysaccharide and glycoside nature. Three important regions highlight their unique chemical structures (3500-2800, 1700-1500, $1200-900 \,\mathrm{cm}^{-1}$) [63]. A wide band around $3300 \,\mathrm{cm}^{-1}$ can be attributed to the hydroxyl group from phenolic (SA) and monosaccharides units (CS and PL) influenced by the hydrogen bond formation. For chitosan, the broad peak at 3313 cm⁻¹ is overlapping the N—H dual bands typically observed for a primary amide. The bands around 2920 cm⁻¹ (presented in the SA and PL) and 2890 cm⁻¹ (presented in the CS) can be attributed to the stretching vibrations of -CH2 and -CH groups, respectively. For the CS, single bands at 1645 cm⁻¹ and 1587 cm⁻¹ are attributed to C-N of chitin residues and to the NH2 bending of the amine groups, respectively [32,65]. For PL and SA, the band around 1640 cm⁻¹ is due to a O-C-O stretching vibration. Bands around 1140 cm⁻¹ represent a polysaccharide (1,4) glycosidic bond stretching vibration [64]. The spectra also show bands at 997 cm⁻¹ (C—O) and at 1348 cm⁻¹ (C-O-H bend) from monosaccharides and carboxylic acid units, respectively [32,66]. A new band at 1714 cm⁻¹ was identified in the control PL-CS crosslinked nanofiber and attributed to the C=O stretching vibration produced by the incorporation of citric acid [37]. The composite nanofibers contain the bands at 755 cm⁻¹ and 929 cm⁻¹ that show the presence of the two primary links in pullulan, the α -(1,4) glycosidic bond, and the α -(1,6) glycosidic bond, respectively [64].

Compared to the uncrosslinked fiber (supplemental S3, the intensity of broad bands around 3305 cm $^{-1}$ for -OH stretching is diminished in the crosslinked fiber, which can be attributed to the formation of acetal bridges due to crosslinking [65]. Identical absorption bands were seen with lower intensity with the addition of SA in the nanofiber. At higher concentrations of SA, the final composites show a slight decrease in their absorption bands at 3298 cm $^{-1}$, 2923 cm $^{-1}$, 1712 cm $^{-1}$, 1635 cm $^{-1}$, 1365 cm $^{-1}$, and 1005 cm $^{-1}$. The intensity of the peaks is lower in PL-CS-SA(H) compared to PL-CS-SA(L). The results reveal that chemical composition of PL, CA, CS, and SA did not undergo substantial change when they were mixed together, so they were able to keep their own properties. It indicates good compatibility of SA in PL-CS composite fiber

The survey XPS of SA and the nanofiber are shown in supplemental

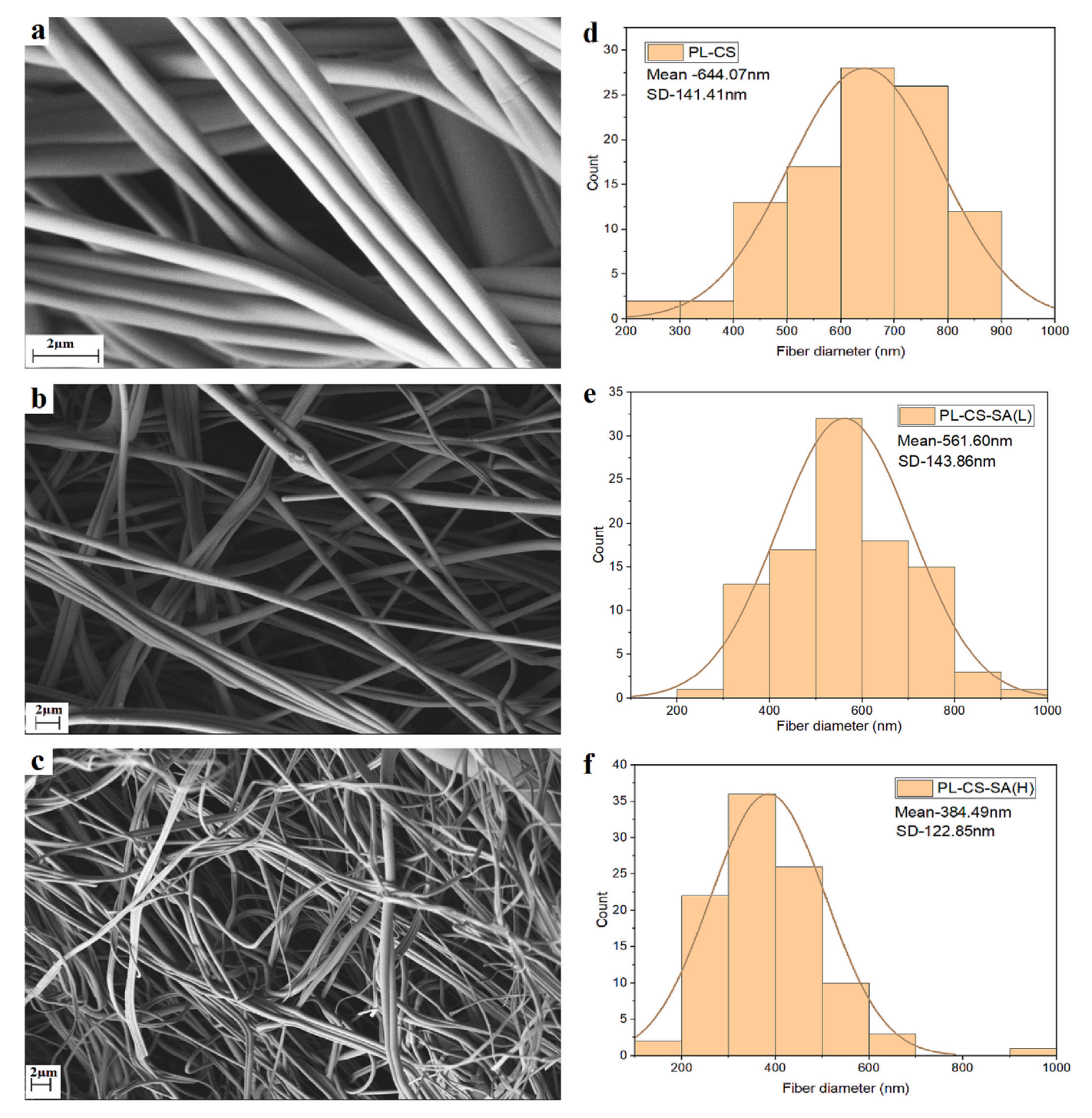


Fig. 2. SEM micrographs of the developed fibrous materials: PL-CS control (a), PL-CS-SA(L) (b), PL-CS-SA(H) (c), and fiber diameter distribution of PL-CS control (d), PL-CS-SA(L) (e), PL-CS-SA(H) (f).

S4. The main elements of PL, CS, CA, and SA are C, N, O, and H. As the amount of CS is very small, a sharp N peak is not clearly visible in the XPS spectra. The C1s peak for SA powder is observed at 286.08 eV. The C1s peaks for PL-CS, PL-CS-SA(L), and PL-CS-SA(H) composite fibers are observed at 287.08 eV, 287.08 eV, and 286.08 eV. The high-resolution C1s spectra of SA and depth profiling of the composite nanofibers are shown in Fig. 4 and supplemental S5. Three XPS spectra were obtained at the depth of 0 nm(surface), 30 nm, and 60 nm of the nanofiber sample. The SA powder shows 5 distinct peaks at 284.08, 285.68,286.48, 287.28, and 288.18 eV, which can be attributed to C-C/C-H, C-OH, C-O-C, C—O, O-C=O, respectively. The CS-PL control fiber

shows 3 distinct peaks at 284.18, 285.78, and 287.18 eV in 30 nm and 60 nm depth which can be attributed to the C-C/C-H, C-OH, and C—O bond, respectively. The PL-CS-SA(L) sample shows 4 distinct peaks attributed to the C-C/C-H, C-OH, C—O, and -COOH bonds. The decreased area under the C—C peak and the increased area under the O-C=O peak in the depth of 60 nm compared to the depth of 30 nm indicate a higher concentration of SA in this region. For PL-CS-SA(H) fiber, the greater area under the peaks at 289.08 eV(-COOH) and 288.78 eV(O-C=O) compared to the area under the peak at 287.58 eV indicates the high concentrations of SA in the fiber.

The thermal stability and effect of SA in the crosslinked composite

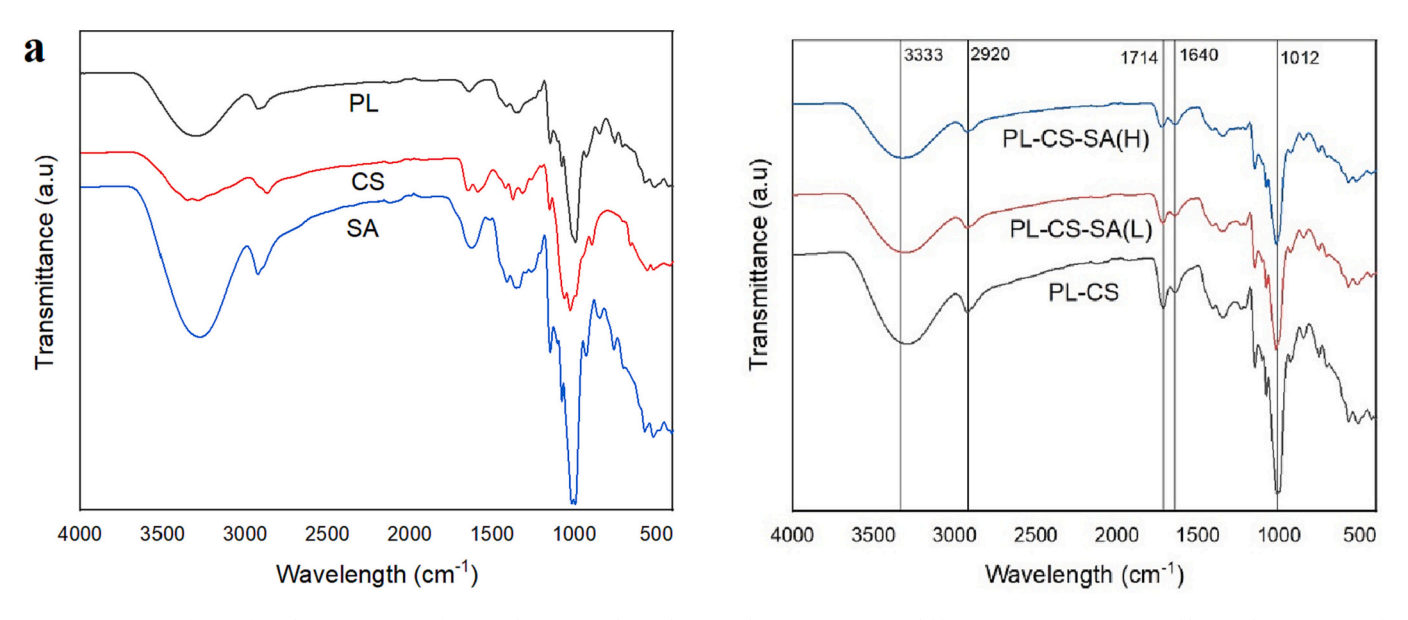


Fig. 3. Fourier transform infrared (FTIR) spectra of PL powder, CS powder and SA powder (a), PL-CS control fiber, PL-CS-SA(L) composite fiber, and PL-CS-SA(H) (b) composite fiber.

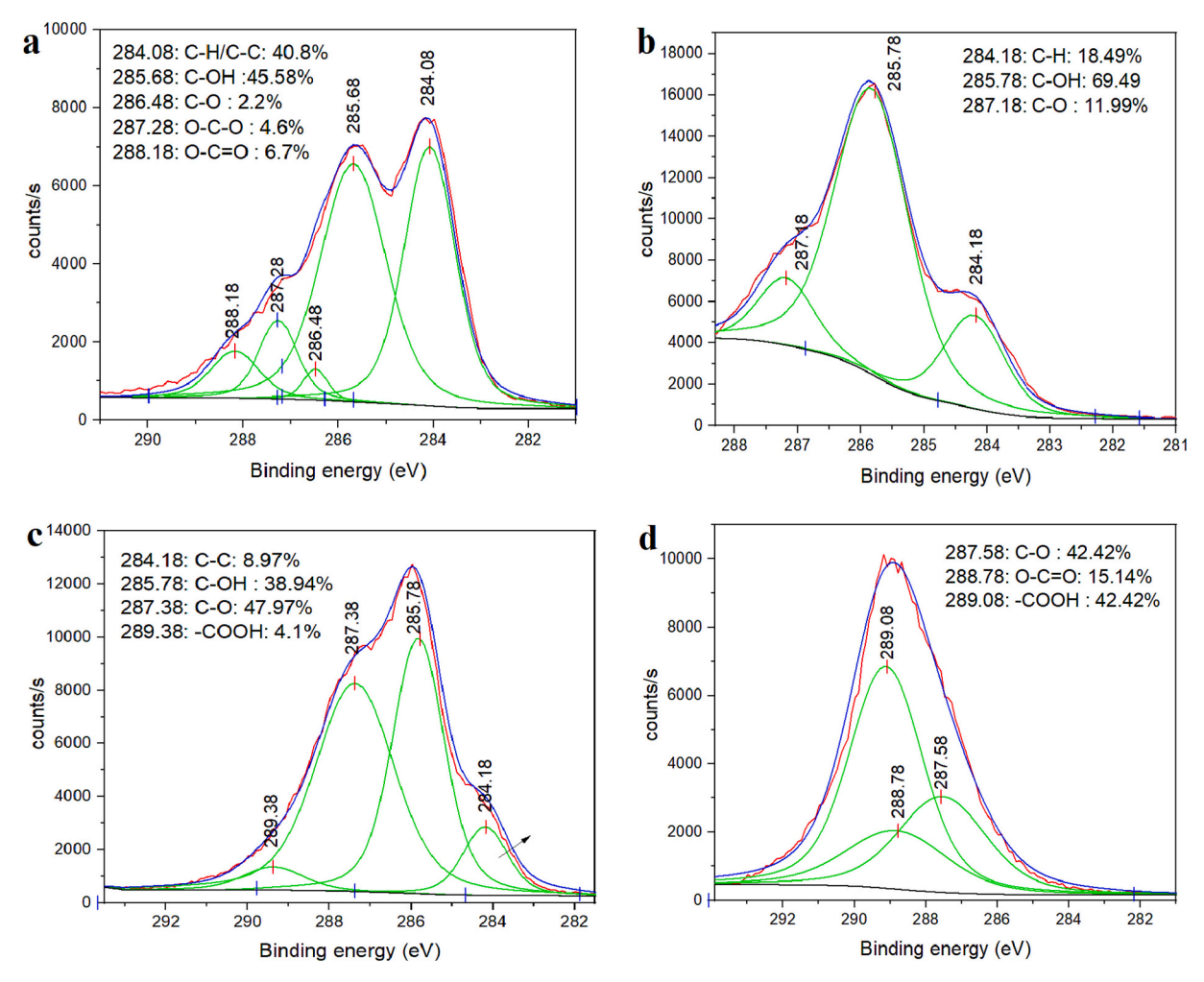


Fig. 4. The high resolution C1s spectra of SA (a), PL-CS control (b), PL-CS-SA(L) (c) and PL-CS-SA(H) (d) fibers at 30 nm depth.

nanofiber membranes were analyzed using a thermogravimetric technique. The TGA and DTG thermograms of the samples are shown in Fig. 5. The SA underwent several degrading stages, beginning with the

loss of water content. In the TGA curve, the first step shows a loss of $8.4\,\%$. The second and third steps are the large-scale degradation of the SA's molecular framework. The onset temperature of degradation for SA is

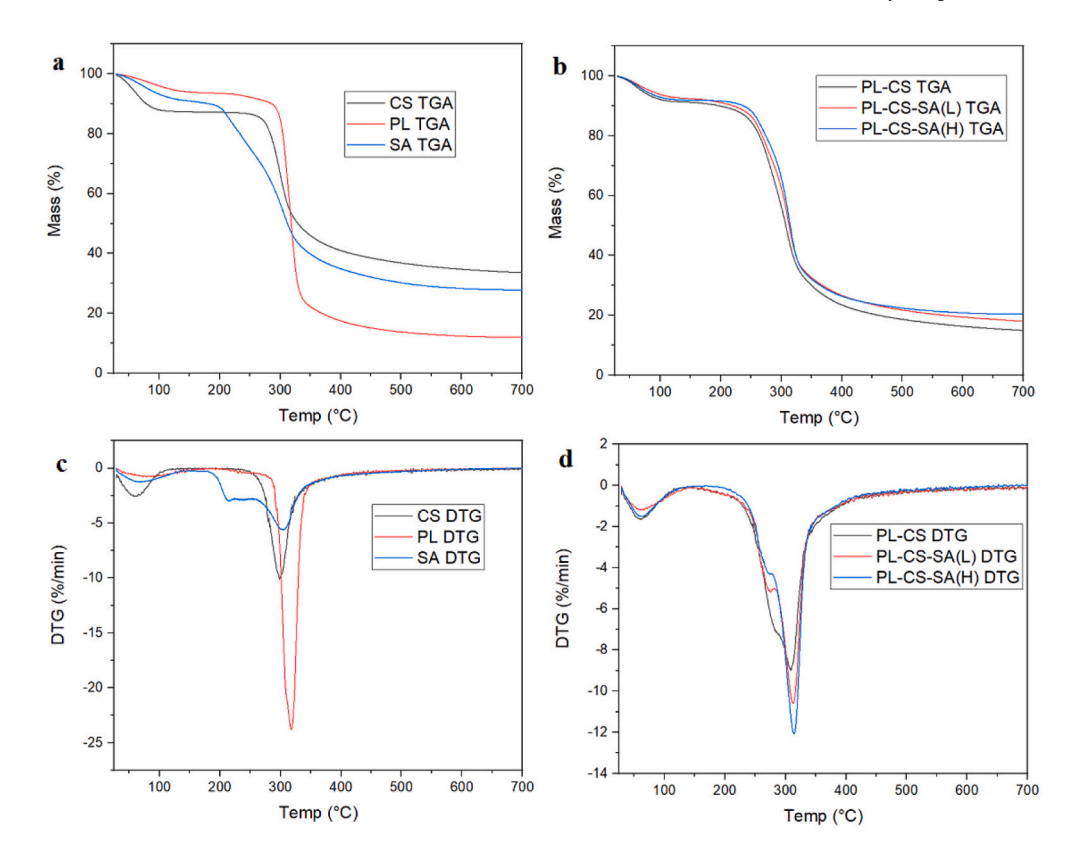


Fig. 5. TGA (a) and DTG (c) analysis of PL, CS, and SA powder samples. TGA (b) and DTG (d) analysis of PL-CS control, PL-CS-SA(L) and PL-CS-SA(H) composite fiber.

 $200~^\circ\text{C}$ followed by a mass loss of 17 %, between $200^\circ\text{-}250~^\circ\text{C}$. This weight loss can be related to the desorption of the hydroxyl group. The third step of degradation between 250 and 700 $^\circ\text{C}$ is due to the degradation of the main molecular skeleton.

From room temperature to 200 °C, pullulan loses around 8 % of its weight, which may have been caused by moisture evaporation (originating from the hydrogen bonds in the exopolysaccharide structure). The onset temperature of decomposition of pullulan is 300 °C. A major weight loss appears between 300 and 330 °C, indicating the degradation of pullulan's chain structure [66]. From the DTG curve, the maximum rate of weight loss is observed at 317 °C.

The control PL-CS composite nanofiber membrane shows degradation over two stages. The first stage is due to loss of water. The second stage was the thermal decomposition of the polymers, starting at 210 $^{\circ}\text{C}$. At this point, the material starts to decompose as a result of the partial breakdown of the molecular structure and the dissolution of intermolecular connections [67]. With the increase of SA content, the nanofiber membranes exhibit a higher onset degradation temperature. It indicates that crosslinking between the PL-CS and SA increased the thermal stability of the nanofiber. The increase in SA content also affects the overall decomposition of the nanofiber samples. For the PL-CS control, PL-CS-SA(L), and PL-CS-SA(H), respectively, residual masses of 14.94 %, 18.07 %, and 20.45 % represent a greater SA concentration in the sample.

Fig. 6 presents the XRD graphs of SA powder, PL-CS control fiber, PL-CS-SA(L) composite fiber, and PL-CS-SA(H) composite fiber. The XRD graph of SA shows two-step peaks at $2\theta=20.8^\circ$ and $2\theta=23^\circ$, indicating that SA consists of semicrystalline (ordered) regions that are dispersed in amorphous (disordered) regions. For PL-CS control sample, the XRD pattern shows no distinct peak indicating the amorphous characteristic nature of this sample. The diffraction peaks of SA disappear in the graph for PL-CS-SA(L), and PL-CS-SA(H), indicating SA stays in a highly dispersed state in PL-CS nanofiber.

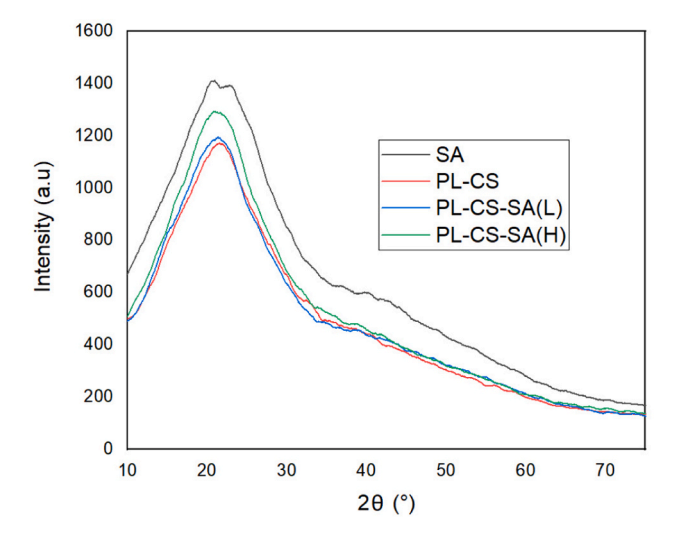


Fig. 6. XRD pattern of SA powder, PL-CS control fiber, PL-CS-SA(L) composite fiber and PL-CS-SA(H) composite fiber.

The controlled release of SA from the fiber membranes was investigated, and the release profiles at 37 $^{\circ}$ C and pH 7.4 are depicted in Fig. 7. The cumulative release profile of SA can be divided into two parts: the initial burst release and the slow sustained release. 33.6 $^{\circ}$ 6 and 38.6 $^{\circ}$ 6 of SA were released in the first hour for PL-CS-SA(L) and PL-CS-SA(H), respectively. The release profile is consistent with the XPS depth profiling result, which shows high concentration of SA in the 30 nm depth from the fiber surface in PL-CS-SA(H) sample. The polymer choice as well as the diffusion and degradation of the polymer have a significant

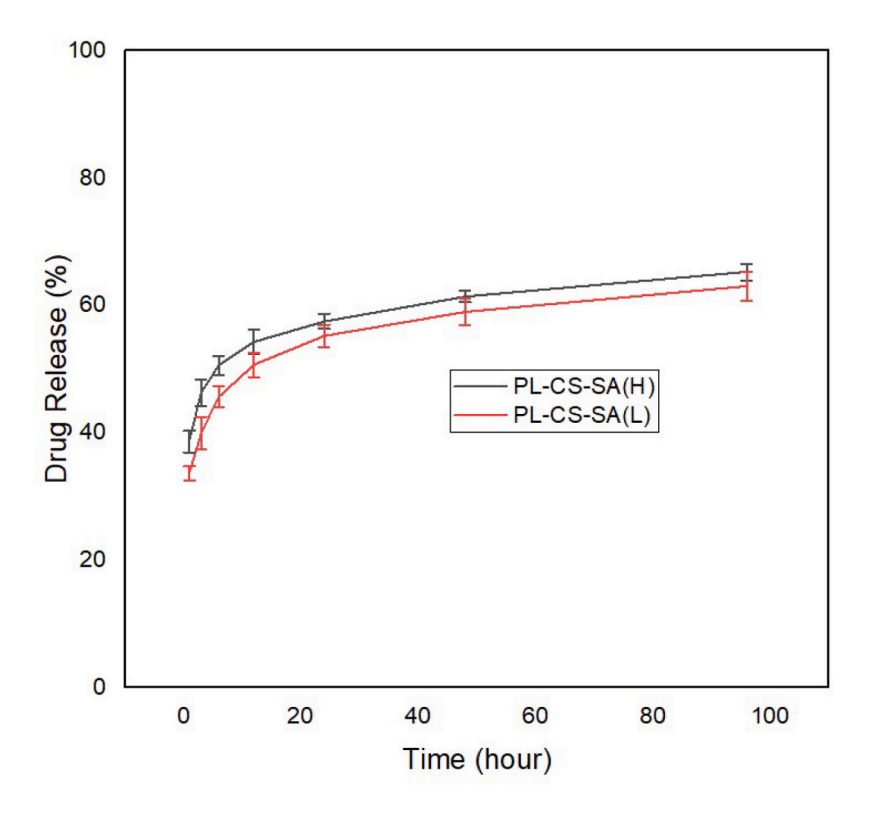


Fig. 7. Drug release profile of PL-CS-SA(L) and PL-CS-SA(H) composite fiber.

impact on the release mechanism of the loaded drug. As both PL and SA are hydrophilic compounds, a burst release is observed during the first hour. SA content could be available at the external surface of these fibers as well as some fraction of PL may not be efficiently crossed-linked with CA. Such a release would be favorable due to the immediate availability of SA at the site of action in order to produce the desired therapeutic effect.

Due to crosslinking of the polymer, it becomes stable in the aqueous medium. As a result, a sustained release pattern is observed. A total drug release of 63.07 % and 65.3 % is observed during the first 96 h. Drug release ideally should be gradual but constant throughout the dosing intervals in order to maintain an adequate therapeutic window of SA for extended time periods. It can be seen from the curve that fittings of all points with zero order ideal curve from t=0 to t=96 h were highly scattered and deviated from ideal points ($R^2=0.6974$ for PL-CS-SA(H) and $R^2=0.6994$ for PL-CS-SA(L)) (Supplementary Fig. S8). However scattering mostly stems from the first 12 h, between 12 and 96 h, the drug release profile is less scattered ($R^2=0.9063$ for PL-CS-SA(H) and $R^2=0.938$ for PL-CS-SA(L)).

To examine the effect of SA on mammalian cell growth, 3 T3 cells were grown in the presence of control PL-CS fibers, as well as SA-containing (SA(L) and SA(H)) fibers (Fig. 8). Strikingly, an MTT assay demonstrated that SA(L) incorporation actually confers improved cell growth, as compared with fibers composed of PL-CS alone. SA(H) fibers do not show a similar increase in cell presence. These results indicate that SA(L) provides an improved environment for cellular growth compared with fibers composed of PL-CS alone, possibly due to buffering the biochemical environment surrounding the fiber matrix.

To evaluate the anticancer properties of SA loaded nanofiber, MTT assay was performed on human colon cancer cells HCT116. The cytotoxic activity of the control fiber (PL-CS) and SA loaded fibers (PL-CS-SA (L) and PL-CS-SA(H)) and bare SA powder is shown in Fig. 9. No inhibition of cell growth is recorded for PL-CS control nanofibers. Nanofiber membranes loaded with SA (PL-CS-SA(L) and PL-SA-SA(H)) show strong cytotoxicity against HCT116 colon cancer cells. The average cell

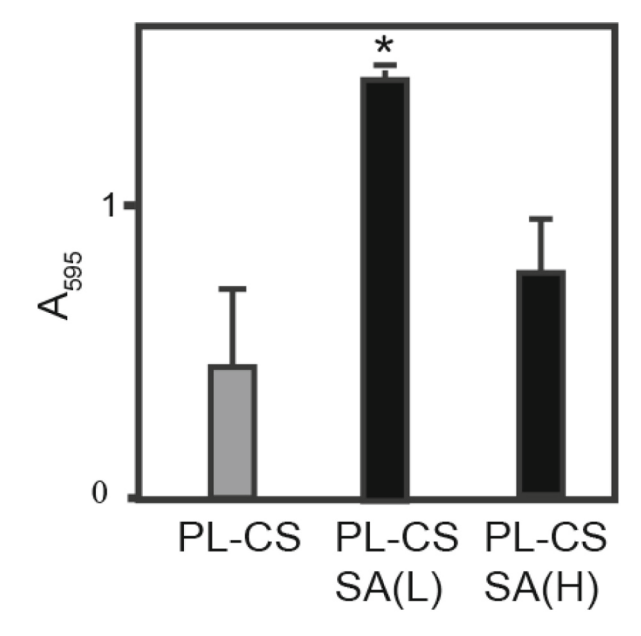


Fig. 8. MTT assay of cell viability in the presence of PL-CS control, PL-CS-SA(L) and PL-CS-SA(H) composite fiber.

inhibition rate for PL-CS-SA(L) and PL-CS-SA(H) is $83.4\,\%$ and $90.3\,\%$, respectively. The results reveal that SA retains its effectiveness after the encapsulation into fiber matrix and is not affected by the forcespinning process.

The nanofiber samples show higher cytotoxicity against HCT116 colon cancer cells compared to bare SA powder. It can be inferred that the polymeric nanofibers acted as a preservative agent for SA, improving its physio-chemical stability and protecting it from premature breakdown. As a result, SA loaded nanofibers show an enhanced activity

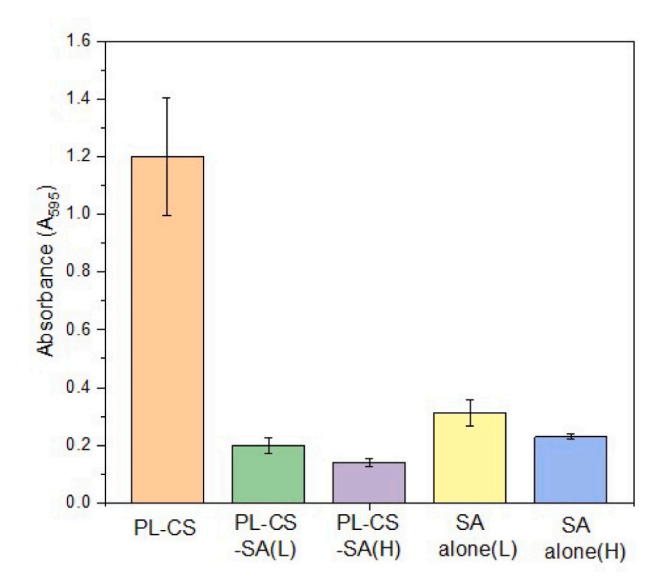


Fig. 9. Anticancer activity of PL-CS control, SA-containing nanofibers, and raw SA-powder.

compared to SA powder. Due to the biodegradability of PL, surgical removal is not necessary once drug release has been completed.

To examine whether the reduction in cell number upon SA treatment was due to cell death, we performed flow cytometric analysis. Cells were grown on control PLCS fibers or with PLCS SA(H) for two days and were then stained with Annexin V-FITC (to examine membrane depolarization) and propidium iodide (PI, to examine membrane permeability), followed by flow cytometric analyses. We found that SA(H) samples had over seven-fold more apoptotic cells compared to control fibers. Only 10 % of HCT116 cells stained positive for PI demonstrating that 90 % of the cells were alive with the PLCS nanofiber (Fig. 10). In contrast, 47 % of the cells were positive for PI, indicative of dead cells in the presence of PLCS SA(H).

4. Conclusion

The successful development of nanofiber membranes composed of Danshen extract containing Salvianolic acid B was achieved using the FS technology. Citric acid was used to crosslink the nanofibrous membranes in order to increased water stability. Increasing concentrations of SA decrease fiber diameter and resulted in long, continuous and homogeneous fibers. Increasing concentration of SA also increased the thermal stability of the nanofibrous membranes. The high surface area makes these systems potential candidate for drug loading in high concentration. Cell-based results indicate that nanofibers containing SA promote cell growth and are not detrimental to the fibroblast cells. The anticancer study revealed that SA loaded nanofiber showed better inhibition to the cell proliferation of HCT116 colon cancer cells. After tumor removal, nanofibers loaded with chemotherapeutic drugs like SA can be placed on the removed tumor site to prevent colon cancer microdeposits from developing. Microdeposits of cancer always remain after surgery and those areas become difficult to penetrate. Once the nanofibers are placed on the tumor site, the membrane will slowly degrade and release the SA. These results suggest that SA-containing nanofibers may provide an innovative strategy for the targeted delivery of anticancer agents in tumor sites.

Future prospective

To expand the use of fibrous membranes in clinical settings, an animal model has been developed as part of the pre-clinical requirements

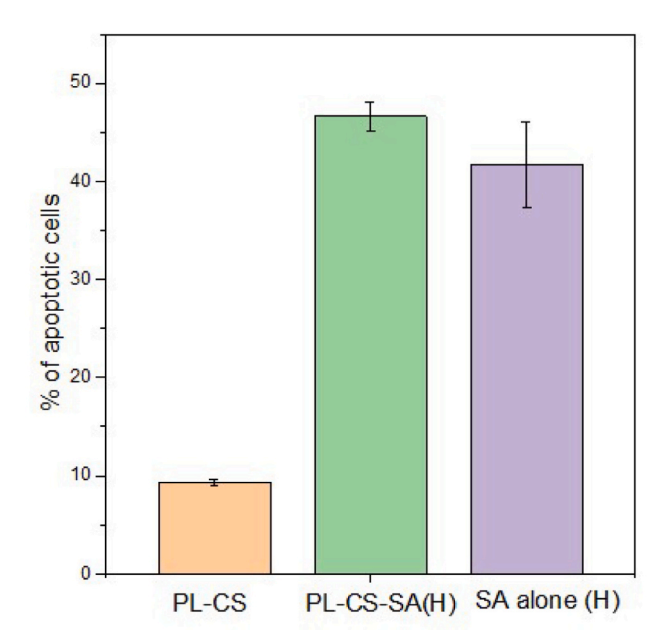


Fig. 10. Flow cytometric analysis of apoptotic cells for PL-CS, PL-CS-SA(H) and SA alone.

to evaluate their in-vivo efficacy, this in collaboration with UTRGV school of medicine.

Ethics approval statement

All cell-based studies were performed with Institutional Biosafety Committee approval from the University of Texas Rio Grande Valley (registration number: 2016–003-IBC).

CRediT authorship contribution statement

S.A., A.A., A.N and K.L. conceived the project. S.A., K.G carried out the experiments. S.A conducted data analysis, and drafted the manuscript. R.G. carried out the cell viability experiments, drafted the cell viability section of the manuscript. M.K conducted the anticancer experiments. M.N.J and N.A.B provided technical support in experiments. V.P. provided technical support on SEM and XPS. V.P., M.K., A.A and K. L. edited the manuscript.

Declaration of competing interest

The authors declare that they have no competing interests or personal/financial contributed conflicts that could influence the work imparted in this manuscript.

Data availability

Data will be made available on request.

Acknowledgment

The authors acknowledge Dr. Jason Parsons for his technical support in PXRD analysis. Authors gratefully acknowledge the support received from National Science Foundation under PREM award DMR 2122178 and partial support by the National Science Foundation through the University of Minnesota MRSEC under Award Number DMR-2011401.

Appendix A. Supplementary data

Supplementary data to this article can be found online at https://doi.org/10.1016/j.jibiomac.2023.126187.

References

- [1] Y. Yao, Y. Zhou, L. Liu, Y. Xu, Q. Chen, Y. Wang, S. Wu, Y. Deng, J. Zhang, A. Shao, Nanoparticle-based drug delivery in cancer therapy and its role in overcoming drug resistance, Front. Mol. Biosci. 7 (2020) 1–14, https://doi.org/10.3389/ fmglb 2020 00193
- [2] T. Nii, Strategies using gelatin microparticles for regenerative therapy and drug screening applications, Molecules 26 (2021) 1–45, https://doi.org/10.3390/ molecules/6/2/6795
- [3] E. Ibrahim, S. Ahmed, S.S.H. Abir, K. Taylor, V.M. Padilla-Gainza, K. Lozano, Centrifugally spun alginate-poly(lactic acid) microbeads: a promising carrier for drug delivery and tissue engineering, Int. J. Biol. Macromol. 220 (2022) 671–682, https://doi.org/10.1016/j.ijbiomac.2022.08.097.
- [4] E. Ibrahim, K. Taylor, S. Ahmed, A. Mahmoud, K. Lozano, Centrifugally spun poly (D,L-lactic acid)-alginate composite microbeads for drug delivery and tissue engineering, Int. J. Biol. Macromol. 237 (2023), 123743, https://doi.org/10.1016/ j.ijbiomac.2023.123743.
- [5] B. Song, C. Wu, J. Chang, Controllable delivery of hydrophilic and hydrophobic drugs from electrospun poly(lactic-co-glycolic acid)/mesoporous silica nanoparticles composite mats, J Biomed Mater Res B Appl Biomater 100 (2012) 2178–2186, https://doi.org/10.1002/jbm.b.32785.
- [6] J. Xu, Y. Jiao, X. Shao, C. Zhou, Controlled dual release of hydrophobic and hydrophilic drugs from electrospun poly (l-lactic acid) fiber mats loaded with chitosan microspheres, Mater. Lett. 65 (2011) 2800–2803, https://doi.org/ 10.1016/j.matlet.2011.06.018.
- [7] D.-G. Yu, L.-M. Zhu, K. White, C. Branford-White, Electrospun nanofiber-based drug delivery systems, Health (Irvine. Calif). 01 (2009) 67–75, https://doi.org/ 10.4236/health.2009.12012.
- [8] J. Xie, C.H. Wang, Electrospun micro- and nanofibers for sustained delivery of paclitaxel to treat C6 glioma in vitro, Pharm. Res. 23 (2006) 1817–1826, https:// doi.org/10.1007/s11095-006-9036-z.
- [9] P.P.G. Guimarães, M.F. Oliveira, A.D.M. Gomes, S.M.L. Gontijo, M.E. Cortés, P. P. Campos, C.T.R. Viana, S.P. Andrade, R.D. Sinisterra, PLGA nanofibers improves the antitumoral effect of daunorubicin, Colloids Surfaces B Biointerfaces 136 (2015) 248–255. https://doi.org/10.1016/j.colsurfb.2015.09.005.
- [10] D. Han, S. Filocamo, R. Kirby, A.J. Steckl, Deactivating chemical agents using enzyme-coated nanofibers formed by electrospinning, ACS Appl. Mater. Interfaces 3 (2011) 4633–4639, https://doi.org/10.1021/am201064b.
- [11] R.S. Singh, N. Kaur, Microbial biopolymers for edible film and coating applications, Adv. Ind. Biotechnol. (2010) 187–216.
- [12] BERNIER, B., The production of polysaccharides by fungi active in the decomposition of wood and forest litter, Can. J. Microbiol. 4 (1958) 195–204, https://doi.org/10.1139/m58-020.
- [13] I.W. Sutherland, Novel and established applications of microbial polysaccharides, Trends Biotechnol. 16 (1998) 41–46, https://doi.org/10.1016/S0167-7799(97) 01130 6
- [14] B.J. Catley, A. Ramsay, C. Servis, Observations on the structure of the fungal extracellular polysaccharide, pullulan, Carbohydr. Res. 153 (1986) 79–86, https:// doi.org/10.1016/S0008-6215(00)90197-6.
- [15] R.S. Singh, G.K. Saini, J.F. Kennedy, Downstream processing and characterization of pullulan from a novel colour variant strain of Aureobasidium pullulans FB-1, Carbohydr. Polym. 78 (2009) 89–94, https://doi.org/10.1016/j. carbool 2009.03.040
- [16] R.S. Singh, G.K. Saini, Pullulan-hyperproducing color variant strain of Aureobasidium pullulans FB-1 newly isolated from phylloplane of Ficus sp, Bioresour. Technol. 99 (2008) 3896–3899, https://doi.org/10.1016/j. biortech. 2007.08.003
- [17] R.S. Singh, N. Kaur, V. Rana, J.F. Kennedy, Pullulan: a novel molecule for biomedical applications, Carbohydr. Polym. 171 (2017) 102–121, https://doi.org/ 10.1016/j.carbpol.2017.04.089.
- [18] R.S. Singh, G.K. Saini, Biosynthesis of pullulan and its applications in food and pharmaceutical industry, Microorg. Sustain. Agric. Biotechnol. 9789400722 (2012) 509–553, https://doi.org/10.1007/978-94-007-2214-9_24.
- [19] K.C. Cheng, A. Demirci, J.M. Catchmark, Pullulan: biosynthesis, production, and applications, Appl. Microbiol. Biotechnol. 92 (2011) 29–44, https://doi.org/ 10.1007/s00253-011-3477-y.
- [20] T. Kimoto, T. Shibuya, S. Shiobara, Safety studies of a novel starch, pullulan: chronic toxicity in rats and bacterial mutagenicity, Food Chem. Toxicol. 35 (1997) 323–329, https://doi.org/10.1016/S0278-6915(97)00001-X.
- [21] O. Pınar, F. Yangılar, P. Oğuzhan, F. Yangılar, Pullulan: production and usage in food industry, African J. Food Sci. Technol. 4 (2013) 57–63.
- [22] B. Mishra, V. Suneetha, K. Rath, The role of microbial pullulan, a biopolymer in pharmaceutical approaches: a review, J. Appl. Pharm. Sci. 1 (2011) 45–50.
- [23] K. Xi, Y. Tabata, K. Uno, M. Yoshimoto, T. Kishida, Y. Sokawa, Y. Ikada, Liver targeting of interferon through pullulan conjugation, Pharm. Res. 13 (1996) 1846–1850, https://doi.org/10.1023/A:1016037225728.
- [24] A. Grenha, S. Rodrigues, Pullulan-based nanoparticles: future therapeutic applications in transmucosal protein delivery, Ther. Deliv. 4 (2013) 1339–1341, https://doi.org/10.4155/tde.13.99.

- [25] U. Hasegawa, S.I.M. Nomura, S.C. Kaul, T. Hirano, K. Akiyoshi, Nanogel-quantum dot hybrid nanoparticles for live cell imaging, Biochem. Biophys. Res. Commun. 331 (2005) 917–921, https://doi.org/10.1016/j.bbrc.2005.03.228.
- [26] R. Nakahashi-Ouchida, Y. Yuki, H. Kiyono, Cationic pullulan nanogel as a safe and effective nasal vaccine delivery system for respiratory infectious diseases, Hum. Vaccines Immunother. 14 (2018) 2189–2193, https://doi.org/10.1080/ 21645515.2018.1461298.
- [27] J.C. Fricain, S. Schlaubitz, C. Le Visage, I. Arnault, S.M. Derkaoui, R. Siadous, S. Catros, C. Lalande, R. Bareille, M. Renard, et al., A nano-hydroxyapatite pullulan/dextran polysaccharide composite macroporous material for bone tissue engineering, Biomaterials 34 (2013) 2947–2959, https://doi.org/10.1016/j.biomaterials.2013.01.049.
- [28] V.W. Wong, K.C. Rustad, M.G. Galvez, E. Neofyotou, J.P. Glotzbach, M. Januszyk, M.R. Major, M. Sorkin, M.T. Longaker, J. Rajadas, et al., Engineered pullulan-collagen composite dermal hydrogels improve early cutaneous wound healing, Tissue Eng. Part A 17 (2011) 631–644, https://doi.org/10.1089/ten.tea.2010.0298.
- [29] R.S. Singh, N. Kaur, M. Hassan, J.F. Kennedy, Pullulan in biomedical research and development - a review, Int. J. Biol. Macromol. 166 (2021) 694–706, https://doi. org/10.1016/j.ijbiomac.2020.10.227.
- [30] M. Rishabha, S. Pranati, B. Mayank, P.K. Sharma, Preparation and evaluation of disintegrating properties of Cucurbita maxima pulp powder, Int. J. Pharm. Sci. 2 (2010) 395–399.
- [31] V. Bansal, P.K. Sharma, N. Sharma, O.P. Pal, R. Malviya, Applications of chitosan and chitosan derivatives in drug delivery, Biol. Res. 5 (2011) 28–37.
- [32] G.A.F. Roberts, Solubility and solution behaviour of chitin and chitosan, Chitin Chem. (1992) 274–329, https://doi.org/10.1007/978-1-349-11545-7_6.
- [33] M. Martínez-Martínez, G. Rodríguez-Berna, I. Gonzalez-Alvarez, M. Hernández, A. Corma, M. Bermejo, V. Merino, M. Gonzalez-Alvarez, Ionic hydrogel based on chitosan cross-linked with 6-phosphogluconic trisodium salt as a drug delivery system, Biomacromolecules 19 (2018) 1294–1304, https://doi.org/10.1021/acs. biomac.8b00108.
- [34] G. Tang, Z. Tan, W. Zeng, X. Wang, C. Shi, Y. Liu, H. He, R. Chen, X. Ye, Recent advances of chitosan-based injectable hydrogels for bone and dental tissue regeneration, Front. Bioeng. Biotechnol. 8 (2020) 1–15, https://doi.org/10.3389/ fbige.2020.587658.
- [35] H. Liu, C. Wang, C. Li, Y. Qin, Z. Wang, F. Yang, Z. Li, J. Wang, A functional chitosan-based hydrogel as a wound dressing and drug delivery system in the treatment of wound healing, RSC Adv. 8 (2018) 7533–7549, https://doi.org/ 10.1039/c7ra13510f.
- [36] F. Xu, B. Weng, R. Gilkerson, L.A. Materon, K. Lozano, Development of tannic acid/chitosan/pullulan composite nanofibers from aqueous solution for potential applications as wound dressing, Carbohydr. Polym. 115 (2015) 16–24, https://doi.org/10.1016/j.carbpol.2014.08.081.
- [37] R. Barbosa, A. Villarreal, C. Rodriguez, H. De Leon, R. Gilkerson, K. Lozano, Aloe Vera extract-based composite nanofibers for wound dressing applications, Mater. Sci. Eng. C 124 (2021), 112061, https://doi.org/10.1016/j.msec.2021.112061.
- [38] Y. Liang, X. Zhao, P.X. Ma, B. Guo, Y. Du, X. Han, pH-responsive injectable hydrogels with mucosal adhesiveness based on chitosan-grafted-dihydrocaffeic acid and oxidized pullulan for localized drug delivery, J. Colloid Interface Sci. 536 (2019) 224–234, https://doi.org/10.1016/j.jcis.2018.10.056.
- [39] G.H. Fard, Z. Moinipoor, S. Anastasova-Ivanova, H.M.N. Iqbal, M.V. Dwek, S. J. Getting, T. Keshavarz, Development of chitosan, pullulan, and alginate based drug-loaded nano-emulsions as a potential malignant melanoma delivery platform, Carbohydr. Polym. Technol. Appl. (2022) 4, https://doi.org/10.1016/j.carpta.2022.100250.
- [40] S. Lin, L. Cui, G. Chen, J. Huang, Y. Yang, K. Zou, Y. Lai, X. Wang, L. Zou, T. Wu, et al., PLGA/β-TCP composite scaffold incorporating salvianolic acid B promotes bone fusion by angiogenesis and osteogenesis in a rat spinal fusion model, Biomaterials 196 (2019) 109–121, https://doi.org/10.1016/j.biomaterials.2018.04.004.
- [41] X.Y. Ji, B.K.H. Tan, Y.Z. Zhu, Salvia miltiorrhiza and ischemic diseases, Acta Pharmacol. Sin. 21 (2000) 1089–1094.
- [42] T. Chen, W.B. Liu, X.D. Chao, L. Zhang, Y. Qu, J.L. Huo, Z. Fei, Salvianolic acid B attenuates brain damage and inflammation after traumatic brain injury in mice, Brain Res. Bull. 84 (2011) 163–168, https://doi.org/10.1016/j.brainresbull.2010.11.015.
- [43] W. Cao, X.W. Guo, H.Z. Zheng, D.P. Li, G.B. Jia, J. Wang, Current progress of research on pharmacologic actions of salvianolic acid B, Chin. J. Integr. Med. 18 (2012) 316–320, https://doi.org/10.1007/s11655-012-1052-8.
- [44] I.S. Lay, C.C. Hsieh, J.H. Chiu, M.S. Shiao, W.Y. Lui, C.W. Wu, Salvianolic acid B enhances in vitro angiogenesis and improves skin flap survival in Sprague-Dawley rats, J. Surg. Res. 115 (2003) 279–285, https://doi.org/10.1016/S0022-4804(03) 00226-9.
- [45] C.S. Liu, Y. Cheng, J.F. Hu, W. Zhang, N.H. Chen, J.T. Zhang, Comparison of antioxidant activities between salvianolic acid B and Ginkgo biloba extract (EGb 761), Acta Pharmacol. Sin. 27 (2006) 1137–1145, https://doi.org/10.1111/j.1745 7254.2006.00378.x.
- [46] L.X. Xie, S.S.K. Durairajan, J.H. Lu, C.L. Liu, W.F. Kum, Y. Wang, I. Koo, W.K. Wu, D. Han, F. Lao, et al., The effect of salvianolic acid B combined with laminar shear stress on TNF-α-stimulated adhesion molecule expression in human aortic endothelial cells, Clin. Hemorheol. Microcirc. 44 (2010) 245–258, https://doi.org/10.3233/CH-2010-1269.
- [47] M. Tang, W. Feng, Y. Zhang, J. Zhong, J. Zhang, Salvianolic acid B improves motor function after cerebral ischemia in rats, Behav. Pharmacol. 17 (2006) 493–498, https://doi.org/10.1097/00008877-200609000-00015.

- [48] Y.H. Chen, G.H. Du, J.T. Zhang, Salvianolic acid B protects brain against injuries caused by ischemia- reperfusion in rats, Acta Pharmacol. Sin. 21 (2000) 463–466.
- [49] Y.H. Liang, P. Li, Q.F. Huang, J. Zhao, X. Liu, M.K. Dai, Salvianolic acid B in vitro inhibited matrix metalloproteinases-1, -2, and -9 activities, J. Chinese Integr. Med. 7 (2009) 145–150, https://doi.org/10.3736/jcim20090210.
- [50] Y. Hao, T. Xie, A. Korotcov, Y. Zhou, X. Pang, L. Shan, H. Ji, R. Sridhar, P. Wang, J. Califano, et al., Salvianolic acid B inhibits growth of head and neck squamous cell carcinoma in vitro and in vivo via cyclooxygenase-2 and apoptotic pathways, Int. J. Cancer 124 (2009) 2200–2209, https://doi.org/10.1002/ijc.24160.
- [51] Y. Zhao, Y. Hao, H. Ji, Y. Fang, Y. Guo, W. Sha, Y. Zhou, X. Pang, W. M. Southerland, J.A. Califano, et al., Combination effects of salvianolic acid B with low-dose celecoxib on inhibition of head and neck squamous cell carcinoma growth in vitro and in vivo, Cancer Prev. Res. 3 (2010) 787–796, https://doi.org/10.1158/1940-6207.CAPR-09-0243.
- [52] L. Zhou, Z. Zuo, M.S.S. Chow, Danshen: an overview of its chemistry, pharmacology, pharmacokinetics, and clinical use, J. Clin. Pharmacol. 45 (2005) 1345–1359, https://doi.org/10.1177/0091270005282630.
- [53] H. Li, L. Shi, J. Wei, C. Zhang, Z. Zhou, L. Wu, W. Liu, Cellular uptake and anticancer activity of salvianolic acid B phospholipid complex loaded nanoparticles in head and neck cancer and precancer cells, Colloids Surfaces B Biointerfaces 147 (2016) 65–72, https://doi.org/10.1016/j.colsurfb.2016.07.053.
- [54] Q. He, J. Zhang, F. Chen, L. Guo, Z. Zhu, J. Shi, An anti-ROS/hepatic fibrosis drug delivery system based on salvianolic acid B loaded mesoporous silica nanoparticles, Biomaterials 31 (2010) 7785–7796, https://doi.org/10.1016/j. biomaterials.2010.07.008.
- [55] E. Shoba, R. Lakra, M.S. Kiran, P.S. Korrapati, Fabrication of core-shell nanofibers for controlled delivery of bromelain and salvianolic acid B for skin regeneration in wound therapeutics, Biomed. Mater. 12 (2017), https://doi.org/10.1088/1748-605X/aa6684
- [56] H. Kuang, Y. Wang, J. Hu, C. Wang, S. Lu, X. Mo, A method for preparation of an internal layer of artificial vascular graft co-modified with Salvianolic acid B and heparin, ACS Appl. Mater. Interfaces 10 (2018) 19365–19372, https://doi.org/ 10.1021/acsami.8b02602.
- [57] R. Siegel, J. Ma, Z. Zou, A. Jemal, Cancer statistics, 2014, CA Cancer J. Clin. 64 (2014) 9–29, https://doi.org/10.3322/caac.21208.

- [58] McGuire S., World Cancer Report 2014. Geneva, Switzerland: World Health Organization, International Agency for Research on Cancer, WHO Press, Adv. Nutr. 2016 (7) (2015) 418–419, https://doi.org/10.3945/an.116.012211.
- [59] Y. Zhang, G. Talmon, J. Wang, MicroRNA-587 antagonizes 5-FU-induced apoptosis and confers drug resistance by regulating PPP2R1B expression in colorectal cancer, Cell Death Dis. 6 (2015) 1–12, https://doi.org/10.1038/cddis.2015.200.
- [60] J. Chen, H. Lu, D. Yan, F. Cui, X. Wang, F. Yu, Y. Xue, X. Feng, J. Wang, X. Wang, et al., PAK6 increase chemoresistance and is a prognostic marker for stage II and III colon cancer patients undergoing 5-FU based chemotherapy, Oncotarget 6 (2015) 355–367, https://doi.org/10.18632/oncotarget.2803.
- [61] Z. Jing, W. Fei, J. Zhou, L. Zhang, L. Chen, X. Zhang, X. Liang, J. Xie, Y. Fang, X. Sui, et al., Salvianolic acid B, a novel autophagy inducer, exerts antitumor activity as a single agent in colorectal cancer cells, Oncotarget 7 (2016) 61509–61519, https://doi.org/10.18632/oncotarget.11385.
- [62] P. Guo, J. Wang, W. Gao, X. Liu, S. Wu, B. Wan, L. Xu, Y. Li, Salvianolic acid B reverses multidrug resistance in nude mice bearing human colon cancer stem cells, Mol. Med. Rep. 18 (2018) 1323–1334, https://doi.org/10.3892/mmr.2018.9086.
- [63] S. Ahmed, M. Keniry, N. Anaya-barbosa, V. Padilla, N. Javed, R. Gilkerson, A. S. Narula, E. Ibrahim, K. Lozano, Oxymatrine Loaded Cross-Linked PVA Nanofibrous Scaffold: Design and Characterization and Anticancer Properties, 2023, pp. 1–10, https://doi.org/10.1002/mabi.202300098, 2300098.
- [64] K.C. Cheng, A. Demirci, J.M. Catchmark, Effects of plastic composite support and pH profiles on pullulan production in a biofilm reactor, Appl. Microbiol. Biotechnol. 86 (2010) 853–861, https://doi.org/10.1007/s00253-009-2332-x.
- [65] H.S. Mansur, C.M. Sadahira, A.N. Souza, A.A.P. Mansur, FTIR spectroscopy characterization of poly (vinyl alcohol) hydrogel with different hydrolysis degree and chemically crosslinked with glutaraldehyde, Mater. Sci. Eng. C 28 (2008) 539–548, https://doi.org/10.1016/j.msec.2007.10.088.
- [66] H. Mirzaee, F. Khodaiyan, J.F. Kennedy, S.S. Hosseini, Production, optimization and characterization of pullulan from sesame seed oil cake as a new substrate by Aureobasidium pullulans, Carbohydr. Polym. Technol. Appl. 1 (2020), 100004, https://doi.org/10.1016/j.carpta.2020.100004.
- [67] K. Lewandowska, Miscibility and thermal stability of poly(vinyl alcohol)/chitosan mixtures, Thermochim. Acta 493 (2009) 42–48, https://doi.org/10.1016/j. tca 2009 04 003